

Understanding the core density profile in TCV H-mode plasmas

D. Wágner, E. Fable¹, A. Pitzschke, O. Sauter, H. Weisen and
the TCV team

Ecole Polytechnique Fédérale de Lausanne (EPFL), Centre de Recherches en
Physique des Plasmas, Association Euratom-Confédération Suisse, Station 13,
CH-1015 Lausanne, Switzerland

¹Max-Planck-Institut für Plasmaphysik, IPP-EURATOM Association
Boltzmannstraße 2 D-85748 Garching bei München, Germany

E-mail: david.wagner@epfl.ch

Abstract. Results from a database analysis of H-mode electron density profiles on the Tokamak à Configuration Variable (TCV) under stationary conditions show that the logarithmic electron density gradient increases with collisionality. By contrast, usual observations of H-modes showed that the electron density profiles tend to flatten with increasing collisionality. In this work it is reinforced that the role of collisionality alone, depending on the parameter regime, can be rather weak and in these, dominantly electron heated TCV cases, the electron density gradient is tailored by the underlying turbulence regime, which is mostly determined by the ratio of the electron to ion temperature and that of their gradients. Additionally, mostly in ohmic plasmas, the Ware-pinch can significantly contribute to the density peaking. Qualitative agreement between the predicted density peaking by quasi-linear gyrokinetic simulations and the experimental results is found. Quantitative comparison would necessitate ion temperature measurements, which are lacking in the considered experimental dataset. However, the simulation results show that it is the combination of several effects that influences the density peaking in TCV H-mode plasmas.

1. Introduction

In recent years numerous works have been devoted to particle transport studies (see the most recent review [1] and references therein). The experimental observations and the theoretical predictions show a good overall agreement. It is now widely accepted that the electron density profile in the core of tokamak plasmas is mainly tailored by turbulent mechanisms. The turbulent state present in the plasma is intimately related to the density peaking and its dependence on the plasma parameters. In this work we apply a unified quasilinear theory of ion temperature gradient (ITG) and trapped electron (TEM) microinstabilities and turbulence [2] that has emerged in the last years to a very specific problem, namely the density profile behaviour in TCV core plasmas. The success of quasi-linear theory in explaining particle transport in TCV L-mode and eITB plasmas

[2, 3] motivates us to test the theoretical predictions against an H-mode dataset as well, using the same methodology. Our goal is to reproduce the observed experimental trends with numerical simulations and understand which transport mechanisms are influential on the density peaking.

Alcator C-Mod internal transport barriers (ITBs) with very strongly peaked density profiles showed density profile flattening with modest electron heating, which was explained by the onset of TEM turbulence, using linear and nonlinear gyrokinetic simulations [4]. The density peaking in the C-Mod ITBs was thought to result from the Ware pinch, with the ITB density gradient during electron heating determined by the balance of Ware pinch and TEM turbulent fluxes, thus acquiring a strong inverse dependence on temperature. In TCV electron ITBs, where transport barriers are seen mainly on the electron temperature profile [5], the density peaking results from a strong thermodiffusive pinch [6] component which can be explained [3] using the quasi-linear model that shall be used in this paper .

The first experiments on TCV with third-harmonic X-mode electron cyclotron resonance heating (X3 ECH) [7, 8] reported reduction of peakedness of the density profile when intense electron heating was applied. A preliminary study [9] of these plasmas concluded that the density peaking is mainly caused by turbulent processes and suggested that the intense electron heating being favourable for TEM destabilization can possibly lead to profile flattening. In recent experimental campaigns of TCV, new data have been collected on ohmic (OH) and ECH H-modes, repeating the very first experiments and also exploring a wide parameter range. These experiments, where special attention was made to the quality of the collected data, allow us to better explore the experimental dependencies and to have more confidence in validation of the theory. The experimental dataset is used to test the quasi-linear model proposed in [2]. Our work is complementary to the recent study with AUG data [10].

In the next section a brief overview of the TCV H-mode experiments is given with a particular attention to the typical parameter ranges within which these plasmas are sustained. In section 3 the theoretical model that is used for the interpretation of the experiments is summarized. In section 4 the results of the simulations are discussed and compared to the experimental observations. Finally, in section 5, general discussion and concluding remarks are given.

2. TCV H-mode plasmas

In TCV ($R = 0.88$ m, $a = 0.25$ m, $I_p \leq 1$ MA, $B_t \leq 1.5$ T, $\kappa \leq 2.8$), L-mode to H-mode transitions are obtained with and without additional heating [11, 12]. The additional heating is provided by powerful third-harmonic electron cyclotron heating system (X3 ECH, 118 GHz, 3×0.5 MW, 2 s, top launch) [7]. In this work we focus on standard ELMy H-modes with type I and type III ELMs with typical ELM frequencies around 35–100 Hz. Time traces of a typical pulse are shown in figure 1. More ‘exotic’ scenarios such as the quiescent ELM-free [8] and snowflake [13] H-mode scenarios are beyond the

3.7	<	$\langle n_e \rangle_{\text{vol}} [10^{19} \text{m}^{-3}]$	<	6.1
0.9	<	$T_e(0) [\text{keV}]$	<	2.5
280	<	$I_p [\text{kA}]$	<	420
1.35	<	$V [\text{m}^3]$	<	1.55
150	<	$P_{\text{OH}} [\text{kW}]$	<	600
250	<	$P_{\text{ECH}}^{\text{inj}} [\text{kW}]$	<	1000
$\delta_{\text{edge}} \approx 0.45, \kappa_{\text{edge}} \approx 1.7, q_{95} \approx 2.4$				

Table 1. Typical parameters of the TCV H-modes.

scope of this present paper and not considered in the analysis.

The experimental database is built on a representative set of sufficiently diagnosed H-mode deuterium pulses. Some typical parameters of these plasmas in the database are shown in Table 1. The dataset contains pulses with OH only and those with additional X3 ECH, the different power levels are relatively well covered. The dataset is somewhat less extended in terms of changes in plasma current and contains plasmas with very similar shape.

The majority ion species is deuterium and the most abundant impurity is carbon, originating from the wall tiles. The typical carbon concentration is a few per cent of the electron density. The effective charge of these plasmas, estimated from soft X-ray measurements [14], is found to be $Z_{\text{eff}} \approx 2$ for all the pulses considered in the analysis, independently on the heating scheme applied. The calculated total (OH plus bootstrap) current, assuming neoclassical conductivity with the measured Z_{eff} value, is consistent with the magnetic measurements.

2.1. Density and electron temperature measurements

The electron density and temperature profiles are measured via Thomson scattering. Density profile measurements are cross-calibrated with the far infrared interferometer (FIR). Typical temperature and density profiles are depicted in figure 2. The radial flux label throughout this paper is $\rho_\psi = \sqrt{(\psi - \psi_0)/(\psi_b - \psi_0)}$, where ψ is the poloidal flux, ψ_0 and ψ_b are the poloidal flux at the magnetic axis and the plasma boundary, respectively. The derivatives of the profiles with respect to ρ_ψ are determined from cubic spline fits. The fit was performed on profiles collected during a stationary phase of pulses, i.e. where the main plasma parameters (plasma current, line averaged density, internal inductance) do not change significantly. The normalized inverse scale length (normalized gradient) of a profile is defined as: $R/L_X = -R \langle |\nabla \rho_\psi| \rangle \partial \log X / \partial \rho_\psi$, where R is the major radius and the $\langle |\nabla \rho_\psi| \rangle$ is the Jacobian of the $r \rightarrow \rho_\psi$ coordinate transformation with r being the distance from the magnetic axis on the outboard midplane. The profiles of the normalized gradients are shown in figure 3.

All the considered pulses exhibited sawteeth. This results in flat average profiles within $\rho_\psi \approx 0.4 - 0.6$ surface, depending on I_p .

2.2. Ion temperature measurements

The C^{6+} ion temperature is measured by charge-exchange recombination spectroscopy (CXRS) [15]. Neutral particle analysers (NPA) [16] provide estimate of the central ion temperature. In these H-mode plasmas, however, due to geometrical constraints, the ion temperature measurements are limited outside $\rho_\psi \approx 0.8$. This fact, strictly speaking, does not allow us to measure the ion temperature profile in the core.

figure 2 b) also shows a typical ion temperature profile between $\rho_\psi = 0.8-1$ overlaid on the electron temperature profiles. The ion temperature does not change significantly when the ECH is applied. From these typical profiles the local value of T_e/T_i at $\rho_\psi = 0.7$ ($\rho_{vol} \approx 0.6$) is around 1 for phases with ohmic heating only, and about 2 for phases with ECH.

The present ion temperature data suggests that the ion temperature gradient is lower than that of the electrons. Assuming the functional form $T_i(\hat{\rho}) (T_e/T_e(\hat{\rho}))^\nu$ for the ion temperature profile, the relation $R/L_{T_i} = \nu R/L_{T_e}$ follows. In figure 2 b) the dashed curve, derived from the electron temperature profile of #40089 using $\hat{\rho} = 0.8$ and $\nu = 0.5$, follows rather well the ion temperature measurements outside $\rho_\psi \approx 0.8$. Following these considerations we estimate R/L_{T_i} to be around 3-5 at $\rho_\psi = 0.7$.

2.3. Collisionality dependence

Statistical analysis of JET [17] and AUG [18] showed that collisionality is the most important scaling parameter for density peaking in H-modes. Both machines report the flattening of the density profile with increasing collisionality. Note that in these machines collisionality is controlled by the combination of neutral beam injection (NBI) heating and ECH. Despite its complexity, collisionality is a frequently used parameter to map parameter dependencies and for inter-machine comparisons. In this subsection the collisionality dependence of the density and temperature profile peaking is presented.

Later (in section 4), the results of the numerical modelling will be presented as a function of the following definition of collisionality:

$$\hat{\nu} = \nu_{ei}/(v_{th}/R), \quad (1)$$

where ν_{ei} is the electron-ion collision frequency, $v_{th} = \sqrt{T_i/m}$ the thermal velocity and R the major radius. In order to facilitate the comparison with previous results the experimental dependences are also plotted as a function of an effective collisionality adopted from [19]: $\nu_{eff} = 0.1n_e Z_{eff} R/T_e^2 (\approx \nu_{ei}/\omega_{De})$, where n_e , T_e are the electron density in 10^{19} m^{-3} and the electron temperature in keV with $Z_{eff} = 2$.

figure 4 shows the normalized logarithmic gradients of the electron temperature (R/L_{T_e}) and density (R/L_n) profiles at $\rho_\psi = 0.7$ as a function of collisionality $\hat{\nu}$ and ν_{eff} . Points around $\hat{\nu} \approx 0.02$, the most typical TCV OH H-mode pulses, have R/L_n around 3. Samples from reversed field campaigns with unfavourable ion ∇B drift direction with somewhat higher density, are located at around $\hat{\nu} = 0.03$ having $R/L_n \approx 3.5$. In the

0.008 < $\hat{\nu}$ < 0.02 range, which is reached by adding 0.5-1.5 MW ECH, R/L_n decreases to about 1.5.

Note that the global trend of R/L_n as a function of the collisionality is very similar to the one observed on FTU fully non-inductive, high density electron heated plasmas [20]. By contrast, H-modes at JET [17] and AUG [10] showed that R/L_n is decreasing with increasing collisionality.

3. Theoretical model

In Ref. [2] a quasi-linear gyrokinetic framework has been proposed for particle transport with which TCV L-mode plasmas and electron internal transport barriers [3] were studied extensively. In this paper we strive to test this model against TCV H-mode data to understand the density profile behaviour. Although there is no general agreement in the community on the applicability of different quasi-linear models, significant effort has been made to compare various models against non-linear simulations [21, 22, 23, 24] and good agreement was found. It was also shown that the fully developed turbulence preserves many features of the linear evolution [22], therefore with an ad-hoc weighting of the linear spectra, non-linear fluxes can be acceptably reproduced [23]. Moreover, quasi-linear predictions fit very well to experimental observations [2, 3, 10]. A relevant exception to this occurs near marginal stability, where a nonlinear upshift of the TEM critical density gradient has been found [4], which increases with collisionality [25]. This effect is clearly outside the framework of quasilinear theory. EC heated experiments are in general not near marginal stability to temperature gradient driven TEMs [26] with $R/L_{T_e} \approx 8$ [27] but may be near marginal stability to longer wavelength density gradient driven TEMs [4]. In our dataset, R/L_n ranges from about 1 to approximately 3.5, with the upper value lying above the density gradient driven TEM threshold (as shown later in figure 5).

We solve the linear gyrokinetic (GK) equation for electrostatic perturbations with a wavenumber $\mathbf{k} = (0, k_y)$ to obtain ω_r^k , γ^k , Γ^k , the real and imaginary part of the mode frequency and the particle flux, respectively, of the most unstable mode. $\omega_r^k > 0$ represents a mode turning in the ion diamagnetic (ITG) direction, while $\omega_r^k < 0$ corresponds to the electron diamagnetic direction (TEM).

ω_r^k , γ^k , Γ^k are evaluated on a range of k_y . We then obtain the quasi-linear fluxes and the average mode frequency of the turbulent state by a weighted average over the mode spectrum:

$$\langle R \rangle = \int_k w_k R^k dk / \int_k w_k dk, \quad (2)$$

where R can stand for Γ^k , q^k , ω^k . The w_k weights are usually chosen according to a quasi-linear rule of the form:

$$w_k = A_0 \left(\frac{\gamma}{\langle k_{\perp}^2 \rangle} \right)^{\xi}. \quad (3)$$

We use the same parameters $\xi = 2$, $A_0 = 1$ as in [2]. We shall discuss effect of this choice later, in section 4.6.

In order to separate the different mechanisms that are responsible for the density peaking, one can decompose the particle flux such as:

$$\Gamma = A \frac{R}{L_n} + B \frac{R}{L_{T_e}} + C, \quad (4)$$

which, assuming stationary plasma and using the zero flux condition when no particle sources are present (as is the case in the core of these ECH/OH plasmas), transforms into

$$\left. \frac{R}{L_n} \right|_{\text{stat}} = -C_T \frac{R}{L_{T_e}} - C_P. \quad (5)$$

The thermodiffusion coefficient $C_T = -B/A$ and the other pinch coefficient $C_P = -C/A$ are evaluated numerically [3, 2].

4. Simulation results

4.1. Setup for the simulations

Linear gyrokinetic calculations have been performed with the initial value flux-tube code GS2 [28]. We introduce two model cases representing TCV OH and ECH H-mode pulses. For both $R/L_{T_e} = 9$, $R/L_{T_i} = 6$, $Z_{\text{eff}} = 2$. For the OH reference case $T_e/T_i = 1.0$, $\hat{\nu} = 0.024$, for the ECH case $T_e/T_i = 2.0$, $\hat{\nu} = 0.008$ (c. f. subsection 2.1).

The magnetic equilibrium of a representative discharge (see figure 1) was calculated by the equilibrium code CHEASE [29]. The $\rho_\psi = 0.7$ flux surface with $q = 1.2$, $s = 0.7$ was used for flux-tube simulations. For the collisions both pitch angle scattering and energy diffusion are taken into account. 13 k_y values are used in the range of $[0.08, 1.6]$ distributed in a logarithmic way. All growth rates and frequencies are normalized to v_{th}^i/R . The binormal wavenumber $k_y \rho_i$ is normalized to ρ_i , the normal wave number is always zero ($k_x = 0$). Note that on the outboard midplane the normal direction is radial. The timestep was fixed to $\Delta t = 0.05$ in units of R/v_{th}^i . 32 grid points for each 2π turn in θ , and 12 poloidal periods were used. The parameters are then scanned according to the various simulation results presented in the next subsections.

4.2. Finding the stationary density gradient

In the absence of core particle sources, as it is the case in the TCV OH/ECH H-modes [30], the stationary value of the density gradient $R/L_n|_{\text{stat}}$ corresponds to the $\Gamma = 0$ condition. Here we only consider the particle flux ascribed to turbulence, we shall deal with neoclassical contributions later, in section 4.5. Other contributions to the total particle flux (e.g. MHD, ripple losses, etc) are neglected. It is also assumed that these approximations hold under both OH and ECH conditions. $R/L_n|_{\text{stat}}$ is obtained by making a set of simulations for different values for R/L_n , keeping all the other input

parameters fixed. At each R/L_n , $\langle \Gamma \rangle$ is evaluated with equation 2. Then the zero point is found by linear interpolation.

In order to understand the relationship between the linear and quasi-linear fluxes, in figure 5 we show the different contributions in equation 2 together with the mode frequency and growth rate of the most unstable mode as a function $k_y \rho_i$ for the OH reference case. First we note that the quasi-linear rule gives small weight at large wavenumbers (short scales), therefore $\langle \Gamma \rangle$ and $\langle \omega_r \rangle$ are mainly determined by the $k_y \rho_i < 0.4-0.5$ wavenumber range (ITG and TEM range).

When the density gradient R/L_n is small (figure 5 a), b)), the most unstable modes are ITGs (positive ω_r), the $w_k \Gamma^k$ contributions to $\langle \Gamma \rangle$ throughout the covered wavenumber range is negative (inwards), making $\langle \Gamma \rangle$ pointing unambiguously inwards. Increasing R/L_n (figure 5 c) and d)), the growth rate of the most unstable modes decreases and at low $k_y \rho_i$, $w_k \Gamma^k > 0$ contributions appear, making $\langle \Gamma \rangle = 0$ when $R/L_n = R/L_n|_{\text{stat}}$ is reached. Further increasing R/L_n (figure 5 e) and f)) the mode frequency changes sign and TEM modes appear at small wavenumbers. When these modes dominate, the particle flux $\langle \Gamma \rangle$ is positive (outwards).

figure 6 shows the quasi-linear particle flux $\langle \Gamma \rangle$ normalized to the total electron heat flux as a function of R/L_n for the two reference cases. Each point in the figure is a result of 13 simulations (averaged over the k_y spectrum as in figure 5). The average mode frequency $\langle \omega_r \rangle$ is also plotted showing that, indeed, the zero flux point is found between ITG and TEM type modes [2]. Note the role of ITG-TEM balance at a certain density gradient in the spectrum and also in adjusting the value of $R/L_n|_{\text{stat}}$. It must also be stressed out, that at the co-existence of different modes, one must certainly account for non-linear effects [4, 25, 24, 31]. It is not expected that the absolute value of $R/L_n|_{\text{stat}}$ from the quasi-linear estimate of the particle flux instantly matches the experimental values; however, its parametric dependence on the plasma parameters is remarkably well retained [2, 3, 10].

4.3. $\nu_{\text{eff}}-T_e/T_i$ scan

We endeavour to reproduce the collisionality dependence reported in Sec. 2.3 with numerical simulations. Since in TCV H-mode experiments collisionality is mainly controlled by intense electron heating, the T_e/T_i ratio certainly increases with additional ECH. It is expected that the temperature ratio has a significant effect on the nature of the dominant instabilities and hence on the particle flux. We also want to explore the effect of the electron-ion collisions at each considered temperature ratio. Therefore, we perform a double parameter scan in the range of $\hat{\nu} = [0.008, 0.012, 0.016, 0.020, 0.024]$ together with a scan in $T_e/T_i = [1, 1.5, 2]$.

The results are summarized in figure 7 a), which shows the predicted value of the density gradient $R/L_n|_{\text{stat}}$ as a function of the collisionality $\hat{\nu}$. Each point is obtained from a scan over R/L_n to determine $R/L_n|_{\text{stat}}$ where $\langle \Gamma \rangle = 0$. Therefore each point in figure 7 is the result of about 10×13 linear simulations. When $T_e/T_i = 1.0$ the predicted

density gradient is decreasing with collisionality. As the temperature ratio is increased, this trend is reversed and at $T_e/T_i = 2.0$ an increase of $R/L_n|_{\text{stat}}$ is predicted with increasing $\hat{\nu}$. These results show a clearer trend (figure 7 b)) if now one plots $R/L_n|_{\text{stat}}$ as a function of $\langle\omega_r\rangle$ which characterizes the nature of the background turbulence and orders very well the predicted values of $R/L_n|_{\text{stat}}$ [2, 10] and also clearly shows that the change in the dominant instabilities alters the collisionality dependence. Therefore, an explanation of the different behaviour of TCV H-modes with respect to JET/AUG plasmas can be due to the different T_e/T_i ratio and hence a different collisionality dependence.

Collisionality provides a purely convective term to the particle flux [1] which is directed outwards for ITG and inwards for TEM modes and increases with increasing collisionality. Intuitively one expects that increasing $\hat{\nu}$ tends to push ω_r towards more positive values [1] (towards ITG type turbulence) due the stabilizing effect of collisions on TEM turbulence [4, 32]. The net effect of collisionality on $R/L_n|_{\text{stat}}$ stems from these two effects: $\hat{\nu}$ influences the turbulence regime and, depending on the turbulence regime, the particle flux. Since an increase in collisionality implies an increase in the real mode frequency the effect of the collisionality on the TEM modes driven outward flux is expected to be weak [1]. Indeed, in figure 7 we observe almost no collisionality dependence at $T_e/T_i = 1.5$, where $\langle\omega_r\rangle \approx 0$. Moving away from this point toward either more positive or more negative $\langle\omega_r\rangle$, the net particle flux is less inwards, and $R/L_n|_{\text{stat}}$ is found at a lower gradient. The increase of T_e/T_i at fixed T_i is destabilizing for ITG and enhances the TEM [33] activity as well. Their interplay is such that TEM takes over rapidly with increasing T_e/T_i , in particular with ECH i.e. by increasing T_e [34]. Indeed, starting from the OH reference point in the ITG instability domain, with increasing T_e/T_i and decreasing $\hat{\nu}$, $\langle\omega_r\rangle$ decreases and the predicted value of $R/L_n|_{\text{stat}}$ is increasing. In the transition region between ITG and TEM, the largest $R/L_n|_{\text{stat}}$ is obtained, then moving towards the TEM domain the density peaking decreases, leaving the point corresponding to the ECH reference case with a very similar $R/L_n|_{\text{stat}}$ value.

We conclude that albeit ECH has a significant effect on the values of $\hat{\nu}$ and T_e/T_i , the change in these parameters only is not sufficient to explain the observed overall experimental behaviour.

4.4. R/L_{T_e} and R/L_{T_i} dependence

It is expected that the temperature gradients have a large effect on the predicted value of the density gradient. As it was pointed out in Sec. 2.2, the ion temperature gradient is generally lower than that of the electrons even at the high collisionality OH plasmas. The ions are even more decoupled from the electrons when intense electron heating is applied. Thus we expect that R/L_{T_i} does not change significantly in these plasmas (more precisely it does not increase). The experimental data are more clear on the R/L_{T_e} dependence; however it is useful to study the dependencies on the parameter, as well.

Two scans of R/L_{T_e} in the range of [6, 7.5, 9, 10.5, 12] have been performed: the first with OH only parameter set ($T_e/T_i = 1.0$, $\hat{\nu} = 0.024$); the second with ECH parameter set ($T_e/T_i = 2.0$, $\hat{\nu} = 0.008$). The other parameters were kept fixed (c. f. Sec. 4.1). In the same way, we change the value of R/L_{T_i} in the range of [4, 5, 6, 7.5, 9].

In figure 8 we present the results of these four scans in terms of $\eta_{ei} = (R/L_{T_e}) / (R/L_{T_i})$. Figure 8 a) shows that the change in R/L_{T_i} has a different effect on the OH and the ECH reference cases. Indeed, starting with the OH reference case (triangles), increasing R/L_{T_i} predicts smaller R/L_n . On the other hand, this parameter has the opposite effect on the predicted peaking for the ECH case. In figure 8 b), it is shown that increasing R/L_{T_e} increases R/L_n for the OH case, while the density peaking is rather insensitive to the change in the electron temperature gradient for the ECH case.

In figure 9 we decompose the predicted R/L_n in terms of C_T and C_P as in equation (5) in order to identify the change in the thermodiffusive and the other contributions. We see that the larger contribution is always the thermodiffusive pinch $C_T R/L_{T_e}$ and usually the two pinches change in the opposite direction and a complicated interplay between the two yields the predicted R/L_n . This means that the parametric dependence of the density peaking is largely determined by the starting reference parameters as mentioned above.

In figure 10 a) we plot these results against $\langle\omega_r\rangle$ which, again, orders very well the simulation results R/L_n [2, 10]. As it was already shown in Sec. 4.3, the OH reference (shaded triangle) case is in the ITG regime ($\langle\omega_r\rangle > 0$), while the ECH (shaded square) reference case is predicted to be more TEM ($\langle\omega_r\rangle < 0$). Increasing the electron temperature gradient results in moving to the left on the $\langle\omega_r\rangle$ axis (towards negative values), while the ion temperature gradient pushes towards larger $\langle\omega_r\rangle$ values. The density peaking is maximal around $\langle\omega_r\rangle \approx 0$ and the predicted value decreases towards both ITG and TEM regime as predicted for eITB and L-mode parameters [3, 2]. We therefore show that this is a very general feature. In figure 10 b) c) we see the thermodiffusive contribution increases towards the ITG regime, while the C_P term decreases. This behaviour of the two pinch terms reinforces their suggested universal role in particle transport [2].

As mentioned in section 2.2, the ion temperature measurements indicate that $(R/L_{T_i}) / (R/L_{T_e}) \approx 0.5$, although we do not have measurements near $\rho_\psi = 0.7$, where we have based our analysis. If this ratio is further decreased in the simulations, moving left in figure 10 a), the value of $R/L_n|_{\text{stat}}$ decreases, following the trend seen previously. However the range of $k_y \rho_i$ where the ITG is the most unstable mode, typically $k_y \rho_i = 0.1 - 0.6$, shrinks and slab-like electronic modes very elongated along the magnetic field lines appear as seen in Refs. [35, 36]. Although their contribution to the particle flux is small, so is that of the remaining ITG and TEM. This domain requires non-linear simulations and the role of non-adiabatic passing electrons to be studied in detail, which is left for further analyses.

4.5. Effect of the Ware-pinch

In ohmic plasmas, the neoclassical Ware-pinch can have significant contribution to the density peaking [4, 37]. The strength of this effect depends also on the heating scheme applied [4, 10]. In the presence of the Ware-pinch, one needs to find $R/L_n|_{\text{stat}}$ from: $\Gamma + n_e W_p = 0$ [4]. In order to cancel normalization factors, it is more convenient to use the Γ/Q_e ratio; therefore, we divide with the electron heat flux Q_e :

$$\frac{\Gamma}{Q_e} + \frac{n_e W_p}{Q_e} = 0. \quad (6)$$

We evaluate the first term using the ratio of the normalized fluxes $\langle \Gamma \rangle / \langle Q_e \rangle$ (which is proportional to $T_e \Gamma / Q_e$) from numerical simulations, while the second term is computed from experimental measurements using $Q_e = Q_e^{\text{exp}}$ and power balance (PB) arguments assuming a stationary plasma, where

$$Q_e^{\text{exp}} = -\chi_e^{\text{PB}} n_e \nabla T_e = \chi_e^{\text{PB}} \frac{R}{L_{T_e}} \frac{n_e T_e}{R}. \quad (7)$$

We find

$$\frac{\langle \Gamma \rangle}{\langle Q_e \rangle} + \frac{R W_p}{\chi_e^{\text{PB}} R / L_{T_e}} = 0, \quad (8)$$

from which one can find the stationary density gradient value with the Ware-pinch effect included. Note that $W_p < 0$. Note also that for any consistent normalization of $\langle \Gamma \rangle$ and $\langle Q_e \rangle$, T_e of equation 7 cancels in equation 8.

We compare the Ware-pinch contribution for the OH and ECH reference cases substituting typical values of W_p and χ_e^{PB} in equation 8, assuming that the intense ECH does not directly drive significant particle flux that must be countered by the turbulent flux to restore the total flux to zero. In figure 11 the ratio of the normalized fluxes $\langle \Gamma \rangle / \langle Q_e \rangle$ without (symbols), and with (no symbols) the Ware-pinch contribution are shown as a function of R/L_n ; (a) shows the OH reference case with $\chi_e^{\text{PB}} = 0.3 \text{ m}^2 \text{ s}^{-1}$, (b) is the ECH reference case with $\chi_e^{\text{PB}} = 1 \text{ m}^2 \text{ s}^{-1}$. For both cases $W_p = -0.3 \text{ ms}^{-1}$. It can be seen that the shape of the $\langle \Gamma \rangle$ curve around $R/L_n|_{\text{stat}}$ can influence the position of the new value of $R/L_n|_{\text{stat}}$. The addition of the Ware-pinch results in a vertical downshift of the curve. At the OH reference case $\langle \Gamma \rangle$ is almost linear with R/L_n . Due to its modest slope, the upshift in $R/L_n|_{\text{stat}}$ can be as large as 1. For the ECH case the slope of the Γ curve is somewhat reduced which would imply a larger change in $R/L_n|_{\text{stat}}$. However, for the ECH case the contribution of the Ware-pinch is negligible mainly because of two reasons. First, the loop voltage decreases as the electron temperature increases at constant current [4]. This reduces the absolute value of W_p . Second, due to the profile stiffness the value of $\chi_e^{\text{PB}} R / L_{T_e}$ is larger in ECH plasmas, which makes the contribution of the second term in equation 8 much smaller.

4.6. Choice of the quasi-linear rule

Our analysis is consistent with the observed experimental data. However it is based on a specific quasi-linear rule (equation 3 with $\xi = 2$). Other similar studies reported

successful interpretations with different quasi-linear theory [10, 23, 21, 38, 22, 3] using different summation rule, or even using only one k_y mode. A question arises whether the results reported here are strongly dependent on the choice of the w weights in equation 2.

We evaluated the quasi-linear fluxes and $R/L_n|_{\text{stat}}$ with several different choices of w for the parameter scans discussed previously. In figure 12 we show again the results of the temperature gradient scans (see figure 10) summing many modes with the power law used thorough this paper and Ref. [2] (squares), summing with the classical mixing-length estimate (diamonds), summing with the exponential rule (triangles) motivated by fluctuation measurements [23], using one mode where the mixing length transport is maximal (circles) [3] and using one mode with $k_y\rho_i = 0.3$ (stars) [10]. Although, the differences in the predicted absolute value of $R/L_n|_{\text{stat}}$ can be as large as 1.5, the relative changes in $R/L_n|_{\text{stat}}$ and the parametric dependencies are nearly identical, independent on the choice of the quasi-linear rule. Figure 12 and 10 show that the main trends do not depend so much on the quasi-linear rule but rather on the main dependence of the underlying most unstable modes. However, it is safer to use the whole spectrum in order to be sure to capture both the effects of ITG and TEM modes. The importance of the most unstable modes explains why similar trends can be expected in non-linear simulations [22, 24, 31] and in the experiments.

5. Conclusions

The collisionality dependence of the local logarithmic electron density gradient R/L_n has been investigated in ohmic and electron cyclotron resonance heated H-mode plasmas on TCV. The density profile flattens when ECH power is added, the normalized density gradient $R/L_n|_{\text{stat}}$ at $\rho_\psi \approx 0.7$ decreases from about 3 to approximately 1.5. The dependence of $R/L_n|_{\text{stat}}$ on collisionality is rather unusual: the density peaking increases with increasing collisionality. With local quasi-linear gyrokinetic simulations it was shown that the change in collisionality alone cannot reproduce the observed experimental behaviour. The simulation results show that the most important parameter is the ion temperature gradient R/L_{T_i} , which was not available in these experiments. Using $R/L_{T_i} = 6$ puts the OH and the ECH reference case in the ITG and the TEM regime, respectively, with predicted $R/L_n \approx 2.5$ and 3. For the OH case the contribution of the Ware-pinch can be as large as $\Delta R/L_n \approx 1$ resulting in a peaking around 3.5 which is in good agreement with the experiments. However, the flat ECH profiles are not recovered. If a lower ion temperature gradient $R/L_{T_i} = 4$ is assumed, the predicted OH density gradient increases to around 4 (with the Ware pinch included) and that of the ECH case decreases to 2. The experimental trends are, therefore, qualitatively explained. The edge ion temperature data suggest that R/L_{T_i} is about 3-5, however new experimental data are required to compare with our simulation results. We have also seen that at very low R/L_{T_i} , below 3-4, electron modes with large $k_y\rho_i$ are seen to play a role, therefore new simulations are also required in this domain with non-

adiabatic passing electrons and non-linear model. The quasi-linear simulations predict that $R/L_n|_{\text{stat}}$ for the OH and the ECH reference case decreases as R/L_{T_i} is decreased, however dedicated experiments are needed to explore how the T_i profile changes between OH and ECH phases.

The simulation results, where the parameters can be changed individually, also show that the collisionality dependence can actually be due to a change in T_e/T_i and $(R/L_{T_e}/R/L_{T_i})$ rather than the collisionality itself. Table 2 summarizes the change in $R/L_n|_{\text{stat}}$ due to the considered parameters.

The $\langle \Gamma \rangle = 0$ stationary condition is set by the balance between ITG and TEM modes as obtained in L-mode simulations [2]. Depending on the turbulence regime, the dependence of $R/L_n|_{\text{stat}}$ on the collisionality, temperature ratios and temperature gradients can be very different, but in all cases the average mode frequency $\langle \omega_r \rangle$ as a figure of merit of the background turbulence clarifies the simulation results. This property of real mode frequency of the most unstable modes was observed in the study of L- and H-mode AUG plasmas [19, 10], L-mode and eITB TCV plasmas [3, 2], and now has been confirmed for TCV H-mode parameters, as well. The neoclassical Ware-pinch can also contribute to the peaking in certain conditions typically when the stationary point lies in an ITG dominated regime and when the electron heat flux is not too large.

It is interesting to relate the present results to those of AUG reported recently in [10]. The density peaking in those considered H-mode plasmas increases with increasing additional ECH power, mainly due to the increase in the ratio of the logarithmic electron temperature gradient to the logarithmic ion temperature gradient and partly also from the increase in the electron to ion temperature ratio. Figure 7. (a) in [10] can be directly compared to the curve with stars in figure 12. In purely NBI heated AUG H-mode plasmas ITG modes are the most unstable modes, positioned on the right part of the plot with positive frequencies. Adding ECH destabilizes the TEMs and $R/L_n|_{\text{stat}}$ increases as the mode frequency decreases. It is predicted that even larger amount of ECH would result in decreasing peaking [10], however, this could not be validated by those experimental results. According to our interpretation, the TCV OH plasmas are positioned very close to the ITG-TEM boundary and the additional ECH moves $R/L_n|_{\text{stat}}$ down on the left branch of the curve in figure 12. Therefore our results combined with AUG observations [10] recover the full non-monotonic $\langle \omega_r \rangle$ dependence.

In these TCV H-mode plasmas, the local behaviour of the density profile can be well explained in a unified quasi-linear gyrokinetic theory of ITG and TEM instabilities and turbulence. This work confirms that the model used to understand particle transport in L-mode [2] and eITB [3] plasmas is also able to reproduce the main trends observed in H-modes. The results of a quasi-linear theory used in this work can be further improved and validated by non-linear simulations and also global codes are expected to predict more precise values of $R/L_n|_{\text{stat}}$. For a better test of this theory, systematic and precise ion temperature profile measurements are desirable. The systematic study of the dependence of local density peaking on the plasma parameters such as collisionality, electron to ion temperature ratio, electron and ion temperature gradient, Ware-pinch

$\hat{\nu}$	0.5	\nearrow	
T_e/T_i	0.5	\searrow	
η	1 – 1.5	ECH \searrow	OH \nearrow
W_p	0.5 – 1	\nearrow	

Table 2. Change in R/L_n when the related parameter increases.

show that the value of the plasma parameters from which these scans are performed are important in order to understand their effects on the stationary value of the density gradient. This complex interdependence is found to be greatly simplified when analysed in terms of the quasi-linear real mode frequency of the most unstable modes.

Acknowledgements

The authors thank M. Kotschenreuther and W. Dorland for having made available the GS2 code. The GS2 simulations have been run on the PLEIADES2 cluster EPFL, Lausanne. This work has been supported in part by the Swiss National Science Foundation.

References

- [1] C. Angioni, E. Fable, M. Greenwald, M. Maslov, A.G. Peeters, H. Takenaga, and H. Weisen. Particle transport in tokamak plasmas, theory and experiment. *Plasma Physics and Controlled Fusion*, 51:124017, 2009.
- [2] E. Fable, C. Angioni, and O. Sauter. The role of ion and electron electrostatic turbulence in characterizing stationary particle transport in the core of tokamak plasmas. *Plasma Physics and Controlled Fusion*, 52:015007, 2010.
- [3] E. Fable, C. Angioni, and O. Sauter. Gyrokinetic calculations of steady-state particle transport in electron internal transport barriers. *Plasma Physics and Controlled Fusion*, 50:115005, 2008.
- [4] D. R. Ernst, P. T. Bonoli, P. J. Catto, W. Dorland, C. L. Fiore, R. S. Granetz, M. Greenwald, A. E. Hubbard, M. Porkolab, M. H. Redi, et al. Role of trapped electron mode turbulence in internal transport barrier control in the Alcator C-Mod tokamak. *Physics of Plasmas*, 11:2637, 2004.
- [5] S. Coda, E. Asp, E. Fable, TP Goodman, O. Sauter, VS Udintsev, R. Behn, MA Henderson, A. Marinoni, GP Turri, et al. The physics of electron internal transport barriers in the TCV tokamak. *Nuclear Fusion*, 47:714, 2007.
- [6] E. Fable, O. Sauter, S. Coda, T. P. Goodman, MA Henderson, H. Weisen, A. Zabolotsky, and C. Zucca. Inward thermodiffusive particle pinch in electron internal transport barriers in TCV. *Plasma Physics and Controlled Fusion*, 48:1271, 2006.
- [7] S. Alberti, G. Arnoux, L. Porte, J.P. Hogge, B. Marletaz, P. Marmillod, Y. Martin, S. Nowak, and the TCV team. Third-harmonic, top-launch, ECRH experiments on TCV tokamak. *Nuclear Fusion*, 45:1224, 2005.
- [8] L. Porte, S. Coda, S. Alberti, G. Arnoux, P. Blanchard, A. Bortolon, A. Fasoli, T. P. Goodman, Y. Klimanov, Y. Martin, et al. Plasma dynamics with second and third-harmonic ECRH and access to quasi-stationary ELM-free H-mode on TCV. *Nuclear Fusion*, 47:952, 2007.
- [9] M. Maslov, H. Weisen, A. Zabolotsky, L. Porte, C. Angioni, M. Beurskens, and the TCV team.

- Density peaking in TCV and JET H-modes. In *Proceedings of the 2006 33rd EPS Conf. on Plasma Physics (Rome)*, volume 301, pages O–3.005, 2006.
- [10] C. Angioni, R.M. McDermott, E. Fable, R. Fischer, T. Pütterich, F. Ryter, G. Tardini, and the ASDEX Upgrade team. Gyrokinetic modelling of electron and boron density profiles of H-mode plasmas in ASDEX Upgrade. *Nuclear Fusion*, 51(2):023006, 2011.
- [11] F. Hofmann, J.B. Lister, W. Anton, S. Barry, R. Behn, S. Bernel, G. Besson, F. Buhlmann, R. Chavan, M. Corboz, et al. Creation and control of variably shaped plasmas in TCV. *Plasma Physics and Controlled Fusion*, 36:B277, 1994.
- [12] Y. Martin, M. A. Henderson, S. Alberti, P. Amorim, Y. Andrebe, K. Appert, G. Arnoux, R. Behn, P. Blanchard, P. Bosshard, et al. Accessibility and properties of ELMy H-mode and ITB plasmas in TCV. *Plasma Physics and Controlled Fusion*, 45:A351, 2003.
- [13] F. Piras, S. Coda, B. P. Duval, B. Labit, J. Marki, S.Y. Medvedev, J. M. Moret, A. Pitzschke, and O. Sauter. “Snowflake” H-mode in a tokamak plasma. *Physical Review Letters*, 105(15):155003, 2010.
- [14] H. Weisen, D. Pasini, A. Weller, and AW Edwards. Measurement of light impurity densities and z_{eff} in jet using x-ray tomography. *Review of Scientific Instruments*, 62(6):1531–1538, 1991.
- [15] A. Bortolon. *Plasma rotation and momentum transport studies in the TCV tokamak based on charge exchange spectroscopy measurements*. PhD thesis, EPFL, 2009. no. 4569.
- [16] A. N. Karpushov, B. P. Duval, C. Schlatter, V. I. Afanasyev, and F.V. Chernyshev. Neutral particle analyzer diagnostics on the TCV tokamak. *Review of Scientific Instruments*, 77:033504, 2006.
- [17] H. Weisen, A. Zabolotsky, M. Maslov, M. Beurskens, C. Giroud, and D. Mazon. Scaling of density peaking in JET H-modes and implications for ITER. *Plasma Physics and Controlled Fusion*, 48:A457, 2006.
- [18] C. Angioni, H. Weisen, O. Kardaun, M. Maslov, A. Zabolotsky, C. Fuchs, L. Garzotti, C. Giroud, B. Kurzan, P. Mantica, et al. Scaling of density peaking in H-mode plasmas based on a combined database of AUG and JET observations. *Nuclear Fusion*, 47:1326, 2007.
- [19] C. Angioni, A.G. Peeters, F. Ryter, F. Jenko, G.D. Conway, T. Dannert, H.U. Fahrback, M. Reich, W. Suttrop, A.U. Team, et al. Relationship between density peaking, particle thermodiffusion, ohmic confinement, and microinstabilities in ASDEX Upgrade L-mode plasmas. *Physics of Plasmas*, 12:040701, 2005.
- [20] M. Romanelli, G. T. Hoang, C. Bourdelle, C. Gormezano, E. Giovannozzi, M. Leigheb, M. Marinucci, D. Marocco, C. Mazzotta, L. Panaccione, et al. Parametric dependence of turbulent particle transport in high density electron heated FTU plasmas. *Plasma Physics and Controlled Fusion*, 49:935, 2007.
- [21] A. Casati, C. Bourdelle, X. Garbet, F. Imbeaux, J. Candy, F. Clairet, G. Dif-Pradalier, G. Falchetto, T. Gerbaud, V. Grandgirard, et al. Validating a quasi-linear transport model versus nonlinear simulations. *Nuclear Fusion*, 49:085012, 2009.
- [22] F. Merz and F. Jenko. Nonlinear interplay of TEM and ITG turbulence and its effect on transport. *Nuclear Fusion*, 50:054005, 2010.
- [23] C. Bourdelle, X. Garbet, F. Imbeaux, A. Casati, N. Dubuit, R. Guirlet, and T. Parisot. A new gyrokinetic quasilinear transport model applied to particle transport in tokamak plasmas. *Physics of Plasmas*, 14:112501, 2007.
- [24] X. Lapillonne, S. Brunner, O. Sauter, L. Villard, E. Fable, T. Görler, F. Jenko, and F. Merz. Non-linear gyrokinetic simulations of microturbulence in TCV electron internal transport barriers. *Plasma Physics and Controlled Fusion*, 53:054011, 2011.
- [25] D. R. Ernst, N. Basse, W. Dorland, C. L. Fiore, L. Lin, A. Long, M. Porkolab, K. Zeller, and K. Zhurovich. Identification of TEM turbulence through direct comparison of nonlinear gyrokinetic simulations with phase contrast imaging density fluctuation measurements. In *Proceedings of 21st International Atomic Energy Agency Fusion Energy Conference, Chengdu, China*, number IAEA-CN-149/TH/1-3, 2006. http://www-pub.iaea.org/MTCD/Meetings/FEC2006/th_1-3.pdf.

- [26] D. R. Ernst, J. Lang, W. M. Nevins, M. Hoffman, Y. Chen, W. Dorland, and S. Parker. Role of zonal flows in trapped electron mode turbulence through nonlinear gyrokinetic particle and continuum simulation. *Physics of Plasmas*, 16:055906, 2009.
- [27] F. Ryter, C. Angioni, M. Beurskens, S. Cirant, GT Hoang, GMD Hogeweyj, F. Imbeaux, A. Jacchia, P. Mantica, W. Suttrop, et al. Experimental studies of electron transport. *Plasma Physics and Controlled Fusion*, 43:A323, 2001.
- [28] M. Kotschenreuther, G. Rewoldt, and WM Tang. Comparison of initial value and eigenvalue codes for kinetic toroidal plasma instabilities. *Computer Physics Communications*, 88(2-3):128–140, 1995.
- [29] H. Lutjens, A. Bondeson, and O. Sauter. The CHEASE code for toroidal MHD equilibria. *Computer Physics Communications*, 97(3):219–260, 1996.
- [30] A. Zabolotsky, H. Weisen, and A. N. Karpushov. Influence of particle sources on electron density peaking in TCV and JET. *Nuclear Fusion*, 46:594, 2006.
- [31] T. Görler, X. Lapillonne, S. Brunner, T. Dannert, F. Jenko, S.K. Aghdam, P. Marcus, B.F. McMillan, F. Merz, O. Sauter, et al. Flux-and gradient-driven global gyrokinetic simulation of tokamak turbulence. *Physics of Plasmas*, 18:056103, 2011.
- [32] C. Angioni, A.G. Peeters, F. Jenko, and T. Dannert. Collisionality dependence of density peaking in quasilinear gyrokinetic calculations. *Physics of Plasmas*, 12:112310, 2005.
- [33] J. Lang, Y. Chen, and S.E. Parker. Gyrokinetic δf particle simulation of trapped electron mode driven turbulence. *Physics of Plasmas*, 14:082315, 2007.
- [34] A. Bottino, O. Sauter, Y. Camenen, and E. Fable. Linear stability analysis of microinstabilities in electron internal transport barrier non-inductive discharges. *Plasma Physics and Controlled Fusion*, 48:215, 2006.
- [35] K. Hallatschek and W. Dorland. Giant electron tails and passing electron pinch effects in tokamak-core turbulence. *Physical Review Letters*, 95(5):55002, 2005.
- [36] C. Angioni, R. Dux, E. Fable, and AG Peeters. Non-adiabatic passing electron response and outward impurity convection in gyrokinetic calculations of impurity transport in asdex upgrade plasmas. *Plasma Physics and Controlled Fusion*, 49:2027, 2007.
- [37] J. Stober, R. Dux, O. Gruber, L. Horton, P. Lang, R. Lorenzini, C. Maggi, F. Meo, R. Neu, J.M. Noterdaeme, et al. Dependence of particle transport on heating profiles in ASDEX Upgrade. *Nuclear Fusion*, 43:1265, 2003.
- [38] M. Maslov, C. Angioni, and H. Weisen. Density profile peaking in JET H-mode plasmas: experiments versus linear gyrokinetic predictions. *Nuclear Fusion*, 49:075037, 2009.

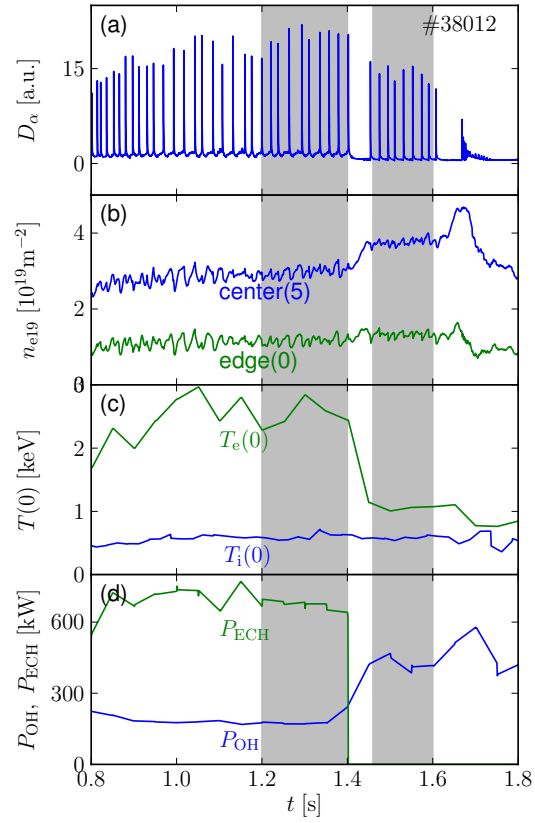


Figure 1. Time traces of (a) D_α emission; (b) central and peripheral FIR chords; (c) central electron and ion (C^{6+}) temperature; (d) OH and ECH power. The stationary profiles are taken from the shaded intervals 1.2–1.4 s and 1.46–1.6 s.

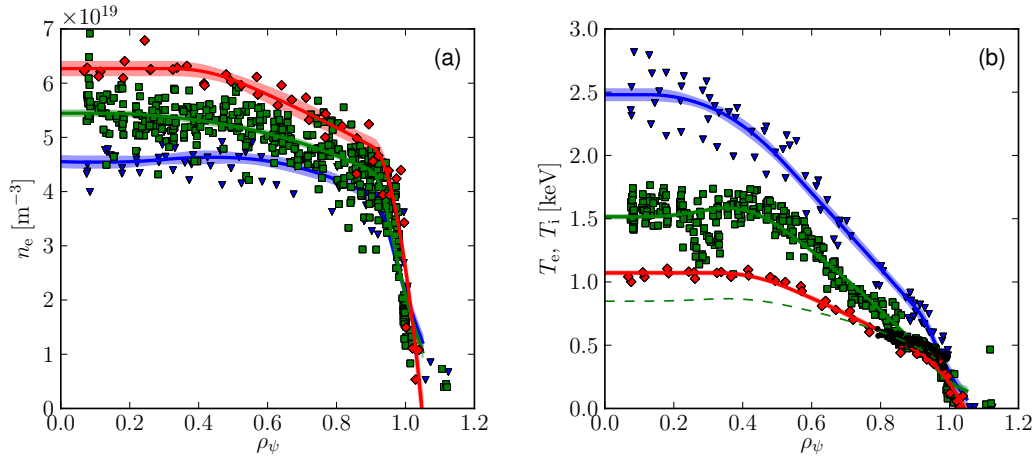


Figure 2. Profiles comparing conditions with ohmic heating only (diamonds, #38012 1.46 – 1.6 s) to those with additional 350 kW (squares, #40089, 0.7 – 1.61 s), 675 kW (triangles pointing down, #38012 1.2 – 1.4 s) ECH. (a) electron density, (b) electron temperature, ion temperature (points, #40089, 0.7 – 1.61 s). Solid lines show the piecewise polynomial fits which were used to compute the gradients. The shaded areas mark the confidence intervals corresponding to 95% confidence level. The dashed line represents $T_i(0.8) (T_e/T_e(0.8))^{0.5}$ (#40089, 0.7 – 1.61 s).

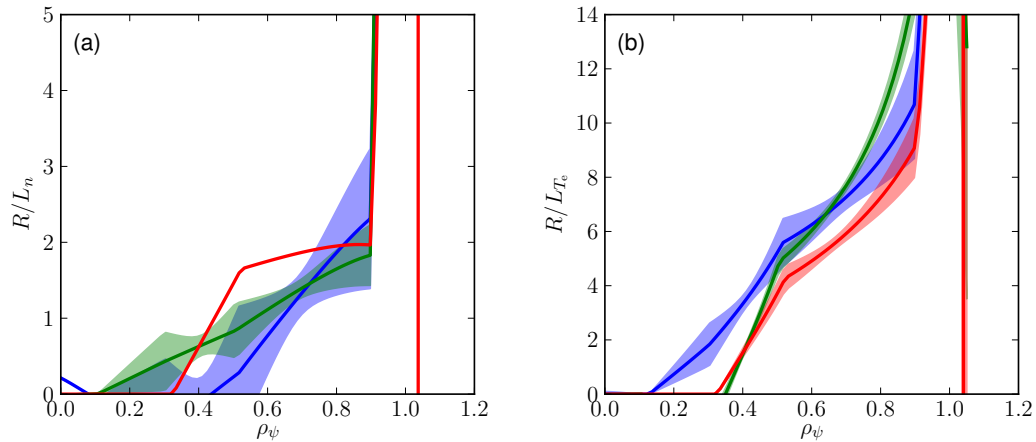


Figure 3. Profiles of the normalized logarithmic gradients calculated from the piecewise polynomial fits depicted in figure 2. The shaded areas mark the confidence intervals corresponding to 95% confidence level.

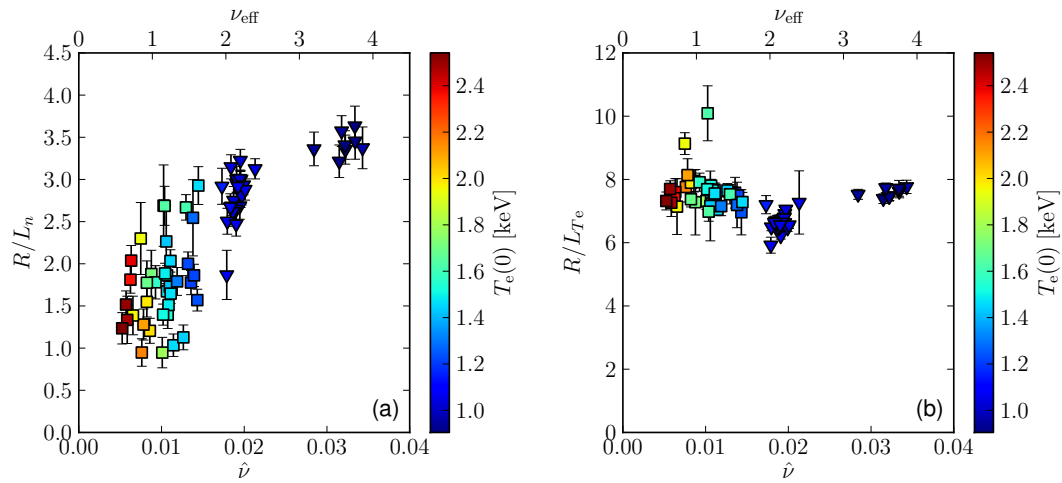


Figure 4. Scatter plots of the normalized logarithmic gradients at $\rho_\psi = 0.7$ as a function of collisionality over the considered database. (a) R/L_n (b) R/L_{T_e} . Different symbols indicate different heating phases, with ohmic heating only (triangles pointing down) and with central X3 ECH (squares). The colorscale (online) represents $T_e(0)$, the central value of the electron temperature.

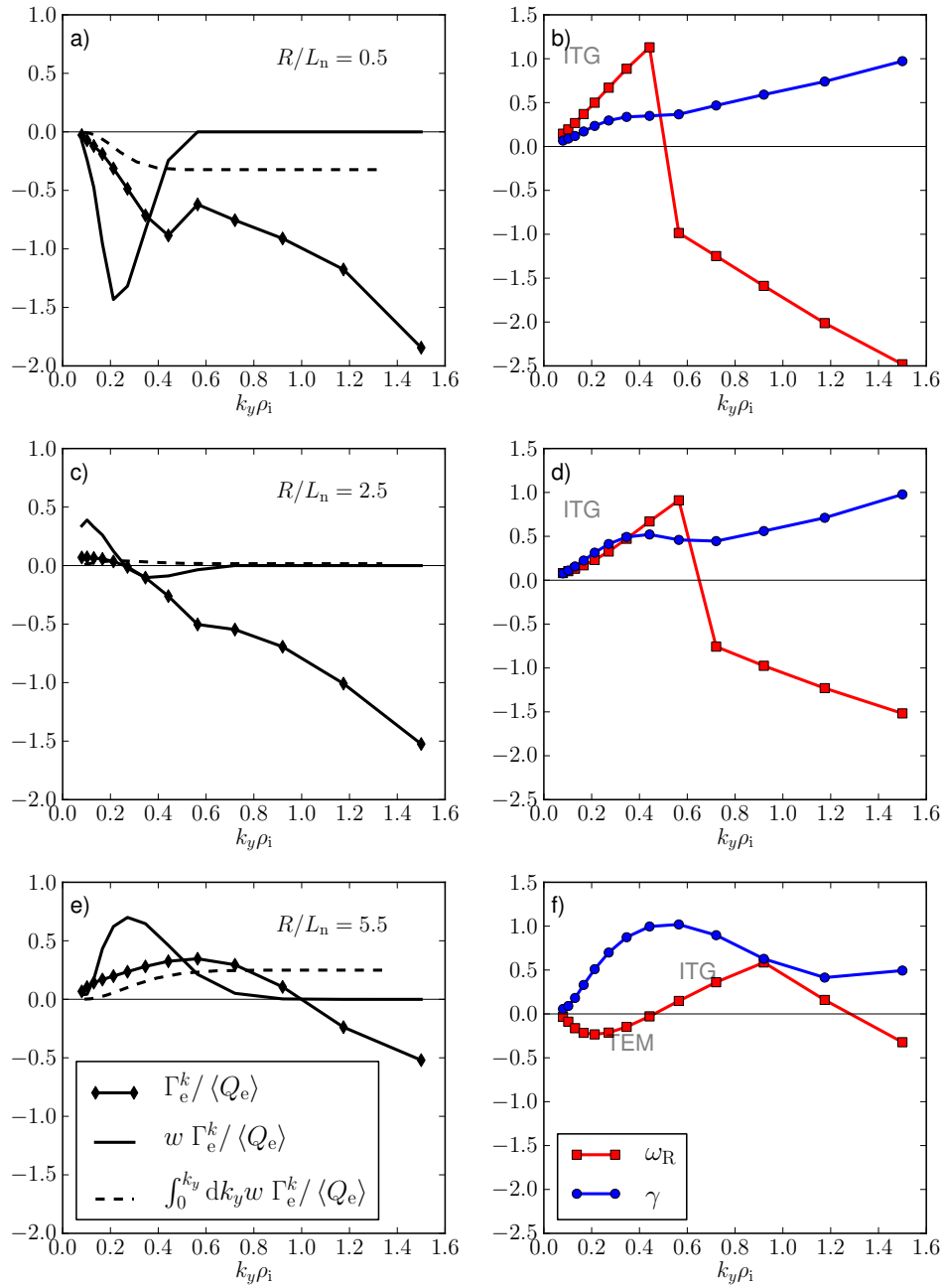


Figure 5. Left: particle flux Γ (diamonds); right: mode frequency ω and growth rate γ (squares and circles, resp.) as a function of $k_y \rho_i$. (a), (b) low R/L_n where ITG is dominant and Γ negative (inwards); (c), (d) $R/L_n \approx R/L_n|_{\text{stat}}$ where $\Gamma \approx 0$; (e), (f) high R/L_n with TEM dominant and positive (outwards) particle flux. The simulation parameters correspond to the OH reference case (see section 4.1).

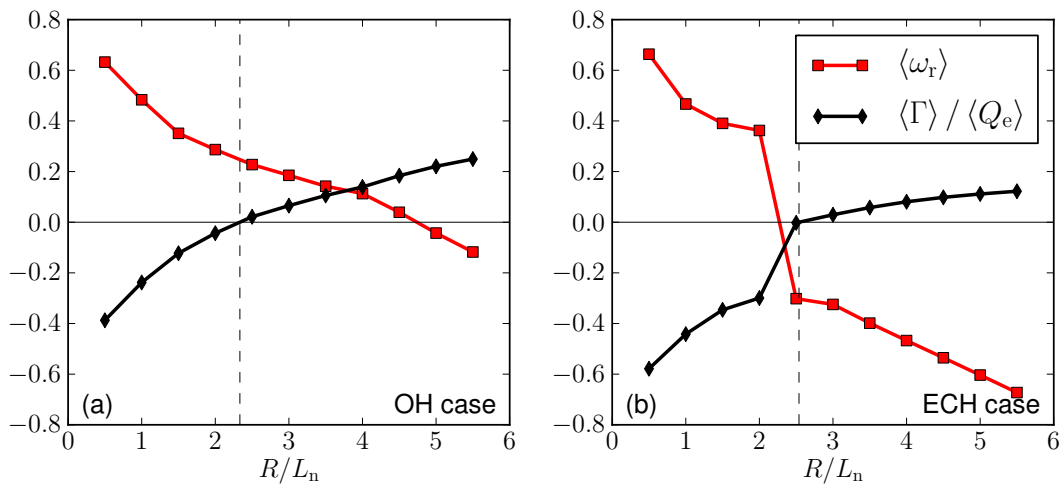


Figure 6. Quasi linear particle flux $\langle \Gamma \rangle$ (diamonds) and average mode frequency $\langle \omega_r \rangle$ as a function of R/L_n (a) OH reference case ($T_e/T_i = 1.0$, $\hat{\nu} = 0.024$), (b) ECH reference case ($T_e/T_i = 2.0$, $\hat{\nu} = 0.008$).

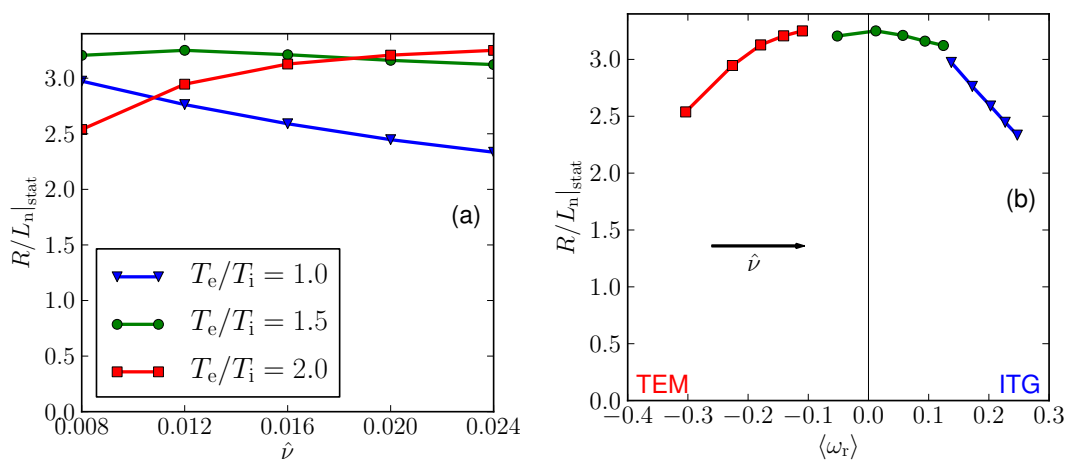


Figure 7. Predicted values of R/L_n for different values of the temperature ratio T_e/T_i , as a function of (a) the collisionality $\hat{\nu}$ and (b) the average mode frequency $\langle \omega_r \rangle$.

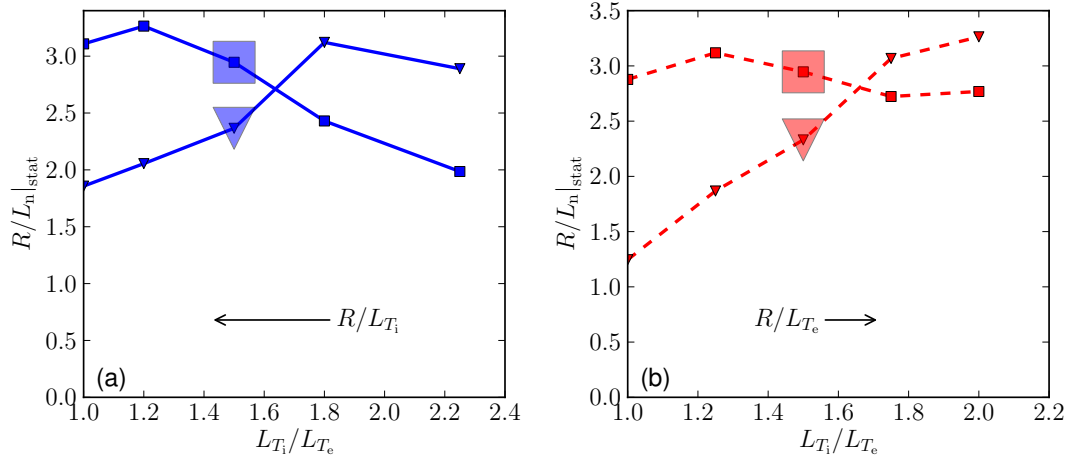


Figure 8. Predicted values of normalized density gradient R/L_n as a function of the temperature gradient ratio L_{T_i}/L_{T_e} changing R/L_{T_i} (solid) and R/L_{T_e} (dashed). Different symbols indicate different heating phases, with OH only (triangles) and ECH (squares). The larger shaded symbols show the reference cases.

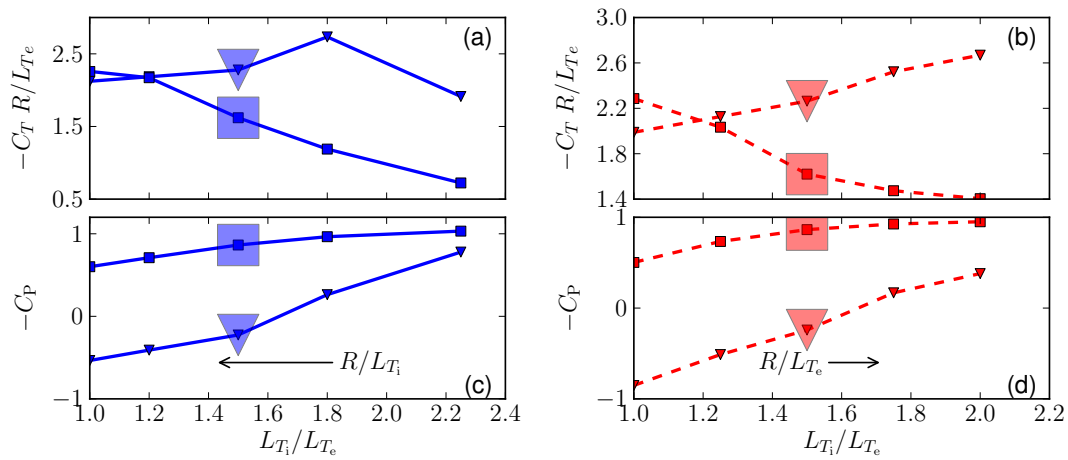


Figure 9. Thermodiffusive $-C_T R/L_{T_e}$ and the other pinch $-C_P$ contributions to the predicted value of R/L_n (c. f. figure 8) as a function of the temperature gradient ratio L_{T_i}/L_{T_e} changing R/L_{T_i} (solid) and R/L_{T_e} (dashed). Different symbols indicate different heating phases, with OH only (triangles) and ECH (squares). The larger shaded symbols show the reference cases.

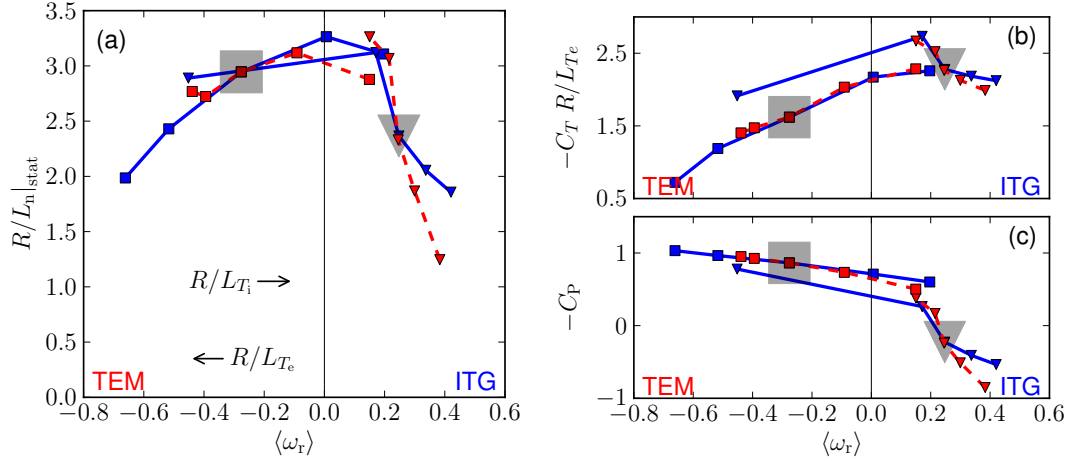


Figure 10. The predicted value of R/L_n , the thermodiffusive $-C_T R/L_{Te}$ and the other pinch $-C_P$ contributions as a function of the average mode frequency $\langle \omega_r \rangle$ changing R/L_{Ti} (solid) and R/L_{Te} (dashed). Different symbols indicate different heating phases, with OH only (triangles) and ECH (squares). The larger shaded symbols show the reference cases.

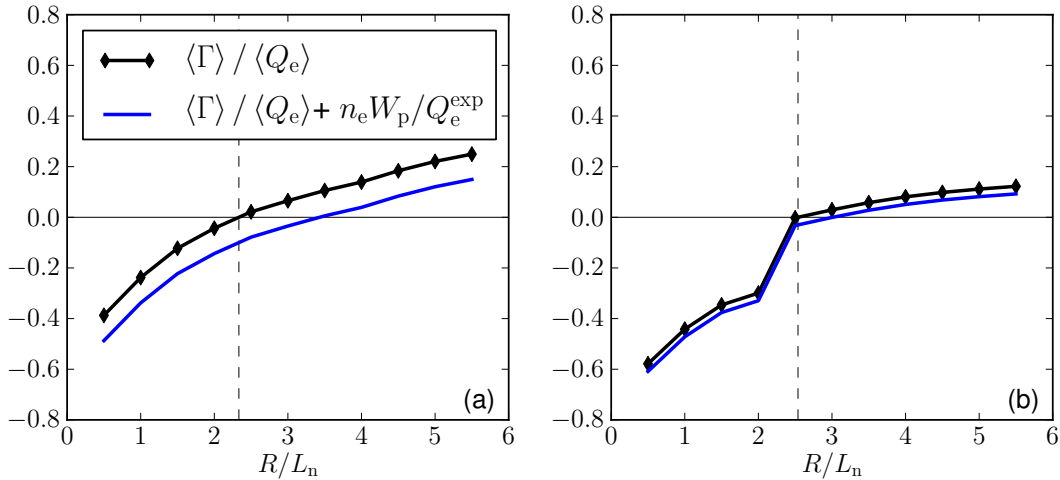


Figure 11. Normalized particle flux as a function of R/L_n , with (no symbols) and without (diamonds) the Ware-pinch contribution according to equation (8): (a) OH model scenario, $\chi_e^{\text{PB}} = 0.3 \text{ m}^2/\text{s}$ (b) ECH model scenario, $\chi_e^{\text{PB}} = 1 \text{ m}^2/\text{s}$. For both cases: $W_p = -0.3 \text{ m/s}$.

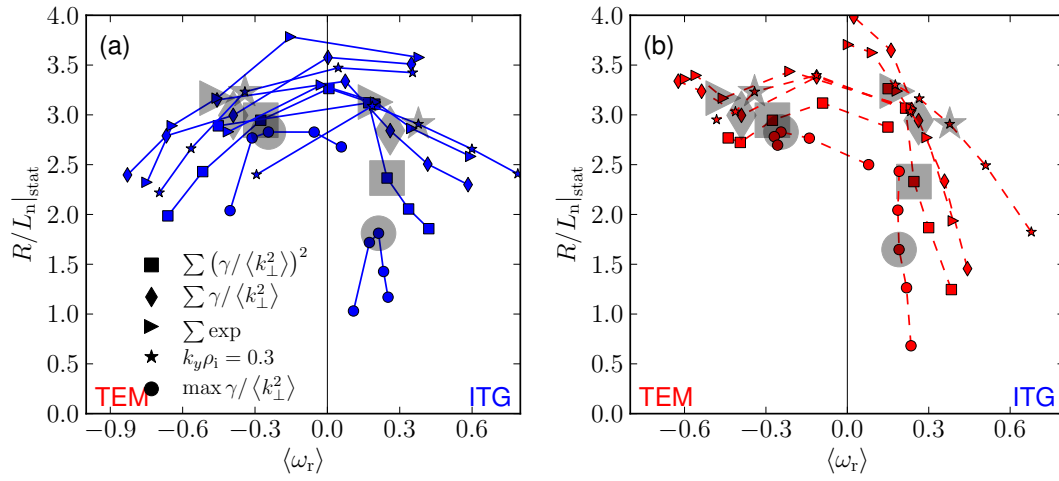


Figure 12. Same as figure 10 (a), using different quasi-linear rules: (a) R/L_{T_i} scan, (b) R/L_{T_e} scan. Different symbols show different prescriptions for the w weights in equation 2. The larger shaded symbols mark the reference cases as in figure 10: the OH case for $\langle \omega_r \rangle > 0$ and ECH case otherwise.